Int J Earth Sci (Geol Rundsch) (2006) 95:1053–1064
DOI 10.1007/s00531-006-0089-3

ORIGINAL PAPER

The growth, collapse and quiescence of Teno volcano, Tenerife: new constraints from paleomagnetic data

R. Leonhardt · H. C. Soffel

Received: 27 June 2005 / Accepted: 6 March 2006 / Published online: 27 April 2006

Abstract Tenerife basically consists of three Miocene shield volcanoes, the Anaga, the Teno and Central shield, as well as the Pliocene Cañadas volcano. The temporal evolution and structural significance of each volcano with respect to the history of Tenerife is still a matter of debate. We present paleomagnetic results in order to enhance the view of the volcanic history of the Teno volcano by means of magnetostratigraphy. It is found that the initial subaerial phase shows reverse magnetizations throughout. After two major sector collapses, dominantly normally magnetized lavas extruded. Comparisons of observed magnetic polarities with the geomagnetic polarity timescale show that these volcanic activities occurred within 0.4 Myr between 6.3 and 5.9 Ma. Significantly younger flows, ~ 5.3 Myr old according to their radiometric age, revealed again normal polarity throughout. The absence of inversely magnetized lavas in-between the two normal periods indicates a volcanic hiatus or erosional phase. The evolutionary sequence and the estimated high production rates for the initial building phase are similar as would be expected for a hotspot volcano. The average geomagnetic field for 6.0 ± 0.2 Ma is close to an axial dipole field showing a slight far-sided/right-handed effect. The field strength, determined by Thellier-type intensity determinations, corresponds to a virtual axial dipole moment of 4.9×10^{22} A m^2. This value is approximately half of the present day field strength, but similar to values obtained for the mid-Miocene. It also corresponds to the proposed tertiary low-field level of the geomagnetic dipole moment.

Keywords Paleomagnetism · Magnetostratigraphy · Absolute paleointensity · Tenerife · Teno volcano

R. Leonhardt (✉) · H. C. Soffel
Department for Earth and Environmental Sciences,
Ludwig-Maximilians-Universität, Munich, Germany
e-mail: leon@geophysik.uni-muenchen.de

Introduction

Despite an enormous amount of geological, geochronological and geochemical data, the origin of the Canary Islands is still debated. A hotspot model akin to the Hawaiian archipelago is favored by a number of researches (e.g., Schmincke 1973; Morgan 1983; Hoernle and Schmincke 1993; Carracedo et al. 1998). Non-plume origins for these islands, however, were also proposed (e.g., Anguita and Hernán 1975, 2000). The hotspot hypothesis is supported by a broad westward decrease in age of the oldest subaerial volcanism on each island (Schmincke 1979; Guillou et al. 2004), rapid magma production during the initial shield stage of Gran Canaria (Mcdougall and Schmincke 1976; van den Bogaard and Schmincke 1998) and structural similarities between Hawaiian Islands and the younger Canary Islands (Carracedo 1999). The geochemical and geophysical signature, however, is less evident (Hoernle and Schmincke 1993; Watts 1994; Anguita and Hernán 2000). This may be partly related to the most prominent difference: in contrast to the Hawaiian Islands, which are located on the fast moving Pacific plate, the Canaries are located on the very slow moving African plate close to the continental margin on old Jurassic crust. Hawaiian Islands, the prototype of hotspot generated islands, are characterized by a

systematic evolutionary sequence. An early shield stage with a rapid production of a high volume of magma is followed by an erosional period and, subsequently, post-erosional magmatism of low production rate (e.g., Langenheim and Clague 1987). With the exception of Gran Canaria, such a temporal change is not apparent on the Canaries. A significant amount of magmatic material, which underplated the flexed oceanic crust below the Hawaiian Islands, is not found at Tenerife (Watts et al. 1997). A further difference between Hawaiian and Canary Islands is the extremely low-rate subsidence of the Canaries (Carracedo 1999). In turn, the almost total absence of subsidence allows for a detailed investigation of evolution, structure and instability of individual island volcanoes.

Tenerife, one of the central islands of the Canary Island chain, is composed of three shield volcanoes, the Anaga, Teno and Central shields, and the Pliocene ''Cañadas series.'' The evolution of Tenerife is characterized by a step-wise growth intercepted by major sector collapses causing giant seaward directed landslides. Remnants of these landslides are found offshore dominantly to the north of Tenerife (Cantagrel et al. 1999; Watts and Masson 2001). The presence of erosional periods on this island, as typically observed on hotspot volcanoes is, however, still a matter of debate. Carracedo et al. (1998) proposed that Tenerife is still in its shield stage. Ancochea et al. (1990) suggested a major erosional phase between 3.5 and 1.9 Ma. Another erosional phase between ~ 9 and 6.5 Ma was proposed by Thirlwall et al. (2000) and Guillou et al. (2004), suggesting that Tenerife is no longer in its shield phase.

The temporal evolution of the Teno volcano (NW-Tenerife) can provide further insight into this problem. Numerous radiometric ages were published for Teno. Magnetostratigraphic investigations provide important additional constraints regarding the temporal evolution of volcanic regions, as has been demonstrated in Iceland (Kristjansson et al. 2003), and also on several Canary Islands (Guillou et al. 1996, 2001). Here, we analyze the past geomagnetic field as recorded in volcanic rocks and provide new clues to better understand the evolution of Teno.

A further important potential of volcanic records of the past geomagnetic field is the possibility to analyze not only the directional field information of inclination and declination, which are needed to establish a magnetostratigraphy, but also the absolute paleointensity. Local investigations of paleomagnetic field strength indicate low values for mid-Miocene rocks from the Canaries, approximately half of the present day field intensity (Leonhardt et al. 2000; Leonhardt and Soffel 2002) and values in the range of the present day field around the last polarity reversal, the 0.78 Ma Matuyama/Brunhes transition (Valet et al. 1999). Such a geomagnetic field intensity difference between the Miocene and the Pleistocene is found globally (Juárez et al. 1998; Selkin and Tauxe 2000; Shcherbakov et al. 2002; Heller et al. 2002). Furthermore, a bimodal distribution of intensities during the geological past appears to be present in the paleointensity database. The low-field mode is characterized by values of about half the present day virtual dipole moment, the high-field mode shows values as observed today (Shcherbakov et al. 2002; Heller et al. 2003). The presence of two preferred states of field strength also require a geomagnetic switching process between those states. The late Miocene rocks of the Teno massif provide an additional point to test for the presence of two different average field states and to pin down the age of the switching process.

Geological setting

Tenerife is the largest and highest island of the Canary archipelago. The geology of this island was extensively studied by Fuster et al. (1968) who defined the main volcano-stratigraphic units, the ''Old basaltic series'' and the ''Cañadas series.'' Carracedo (1979) extended those studies by geochronological and magnetostratigraphic data, specifying the three main volcanoes of the Old basaltic series of Tenerife, the Anaga, Teno and Central shield. The subaerial evolution of the island began approximately 12 Myr ago with the formation of the Central shield (Thirlwall et al. 2000; Guillou et al. 2004). Remnants of the 12–9 Ma activity are found in the Roque del Condo massif, SW-Tenerife, and in numerous water tunnels excavated for groundwater mining (Carracedo 1999). After a ~ 3 Ma period of quiescence, the Teno volcano located in NW-Tenerife, rose above sea level (Guillou et al. 2004). The Anaga volcano in NE-Tenerife formed between 5 and 3.5 Ma (Guillou et al. 2004). The latest Cañadas series was essentially built between 1.9 and 0.2 Ma (Ancochea et al. 1990) dominantly in the central part of the island with its most prominent member, the 3,718 m high stratovolcano Pico de Teide. Episodes of volcanic growth were interrupted by sector collapses producing seaward directed landslides and possibly giant tsunamies. It was suggested that locations of growth and collapse are controlled by the geometric arrangement of the overlapping volcanic edifices (Walter 2003). Several flank collapses are documented forming submarine landslide deposits covering

thousands of square kilometers (e.g., Watts and Masson 2001).

The Teno massif is characterized by rough landscape. Deep canyons (''barrancos'') with up to 200 m vertical side walls, high scarps and cliffs are typical for this strongly eroded region. The occurrences of the Miocene Old basaltic series are shown in Fig. 1. Two subseries termed the lower and upper sequence were previously defined considering a prominent angular unconformity (Ancochea et al. 1990). Walter and Schmincke (2002) recognized two polymict debris deposits forming angular unconformities which mark two giant sector collapses during the evolution of the Teno volcano (Fig. 1). The authors defined three subseries: (1) the Los Gigantes Formation (LGF), (2) the Carrizales Formation (CF) which formed after the Los Gigantes collapse by replenishing the scarp and (3) the El Palmar Formation (EPF) which filled the Carrizales collapse (CC) scarp. However, based on radiometric age determinations and magnetostratigraphy Guillou et al. (2004) demonstrated that this previously defined LGF did not completely form before extrusion of the EPF. Significantly younger rocks, compared to EPF, are found in the Los Gigantes cliffs. The younger rocks are hereinafter termed to represent the LGF. Lavas formed before the CF and EPF collapses are exposed in the Barranco de Masca and are referred to as Masca Formation (MF). The first collapse, dividing MF and CF, will be referred to as the Masca collapse (MC). K–Ar ages of Guillou et al. (2004), combined with Ar–Ar data from Thirlwall et al. (2000), point to volcanic activity in Teno from 6.4 to 6 Myr. Previous ages (Ancochea et al. 1990) suggest a slightly longer volcanic activity from 6.7 to 4.5 Myr, possibly interrupted by an erosional period. Our paleomagnetic investigation aims to provide additional constraints to the temporal evolution of the Teno volcano.

Experimental procedures

Paleomagnetic samples were obtained from 25 lava flows of Old basaltic series (Fig. 1). At least four separate oriented samples were taken from each lava flow using a portable drill. Whenever possible the cores were drilled in the middle of the flow with a spacing of 1–2 m between different cores. Both magnetic and sun compass were used for orientation. Lightning strike remagnetized lavas were avoided by checking the deflection of the compass needle. Successive flows were only sampled in profile P between sites P-1 and P-10 (Fig. 1).

Measurements and demagnetization of the natural remanent magnetization (NRM) were performed in the magnetically shielded room at the paleomagnetic laboratory of the University of Munich in

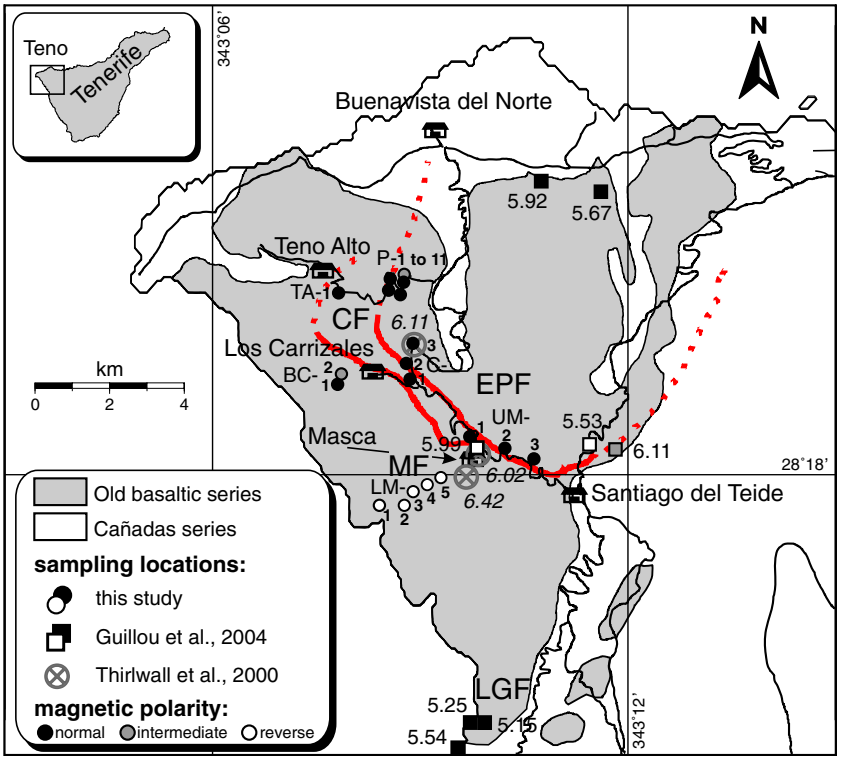

Fig. 1 Simplified geological map of the Teno region, Tenerife. Paleomagnetic site locations of this study and their magnetic polarities are shown as *circles*. Site locations of Guillou et al. (2004) and magnetic polarity are given in *boxes*. The corresponding K/Ar age is written in *normal typeface*. Sampling locations of Ar/Ar dated flows of (Thirlwall et al. 2000) are marked by *grey encircled crosses* and their corresponding age is printed *italic*. The outlines of the paleo-scarps identified by Walter and Schmincke (2002) are shown by *thick solid lines* (found) and *dotted lines* (inferred)

Niederlippach. Remanence measurements were carried out using a Molspin spinner magnetometer and a DC 2G cryogenic magnetometer for weakly magnetized samples. On average, one half of the samples were treated thermally up to 600°C and the other half with alternating field (AF) demagnetization up to 150 mT using at least ten demagnetization steps. For the majority of the lava flows thermal and AF demagnetization were equally effective for determining the characteristic remanent magnetization of the samples. The demagnetization data were analyzed using principle component analysis.

Samples from different lava flows were used for a set of standard rock magnetic measurements. Isothermal remanent magnetization–acquisition, backfield curves, hysteresis loops at room temperature and thermomagnetic curves (applied magnetic field B = 100 mT, maximum temperature T_{max} = 600°C) were measured for each of these samples using a variable field translation balance. Determination of the anisotropy of the magnetic susceptibility (AMS) was done on a KLY2. All paleointensity determinations were conducted in a MMTD20 thermal demagnetizer. Most of the measurements were performed in an argon atmosphere on minicores with an diameter of 5 mm. Two specimens, 223-1A and 223-1C, had standard inch size and were treated in air, yielding a similar success rate and similar results as the minicores from the same site (Table 2). Minicores were taken unoriented from the lower part of individual drill cores and the primary character of the direction was ascertained by demagnetization of sister specimens from the same drill core. Due to their small size, the orientation of the specimens in the sample holder along the x and y-axis within the cryogenic magnetometer is afflicted with slightly higher deviations, leading to a more scattered declination information than for inch specimens. The acquisition of partial thermoremanent magnetization (pTRM) along the sample's z-axis, however, was accurate within 1°. Therefore, vector subtraction for the analysis of minicore determinations can be performed exclusively along the z-axis. The major advantage of using minicores stems from a reduced time for each heating cycle and the use of a larger collection of samples within one measurement run which are all centered in the furnace, guaranteeing a small temperature gradient. Laboratory fields of 20–38 μT applied during heating and cooling were used for all measurements. Field accuracy is 0.1 μT.

For site M-4, four specimens, 2 in. specimens of one drill core and two minicores of one drill core, were measured using two different modifications of the Thellier method, MT1 and MT2, respectively. MT1 refers to experiments with demagnetization at a given temperature prior to acquisition of a pTRM at the same temperature. The inverse treatment, ''in-field'' measurement before zero-field measurement, is termed MT2. MT2 experiments enable one to identify components of magnetization acquired during the field-on step which are not removed by thermal demagnetization to the same temperature, either due to alteration or multidomain (MD)-tails. All other paleointensity determinations were performed with the modified Thellier-technique MT4, which is a zero-field first method incorporating pTRM checks, additivity checks (Krása et al. 2003) and pTRM-tail checks (Riisager and Riisager 2001) evaluated with respect to the directional difference between applied field and NRM according to Leonhardt et al. (2004b). pTRM checks were conducted for all methods in-field after the demagnetization step. Fourteen samples of the collection were analyzed using corrections for magnetomineralogical changes (Valet et al. 1996; Leonhardt et al. 2003). This method uses the cumulative difference of pTRM checks for correcting alteration which affects blocking/unblocking temperatures below the heating step of the check. An important prerequisite for applying this method is the proven absence of MD remanence. In addition to curved diagrams, MD effects also lead to biased pTRM checks (Leonhardt et al. 2004b), whose differences to the pTRM value are used for correcting magnetomineralogical changes. In the case of our experiments, the absence of MD remanence was tested by pTRM-tail checks and additivity checks. If correction is successful, additivity checks should fall on the associated pTRM values and, therefore provide a meaningful test regarding the quality of the correction. All paleointensity determinations were analyzed using the ThellierTool software (Leonhardt et al. 2004a). For characterizing the quality of absolute paleointensity determination the criteria of Leonhardt et al. (2004a) were applied.

Results

Paleodirectional analysis

A primary characteristic component of magnetization could be unambiguously identified in 92% of the samples. Viscous overprints yielding the present day magnetic field direction were observed, but these could usually be removed at demagnetization steps below 200°C or 20 mT, respectively (Fig. 2). A few samples with unstable directions were excluded from further

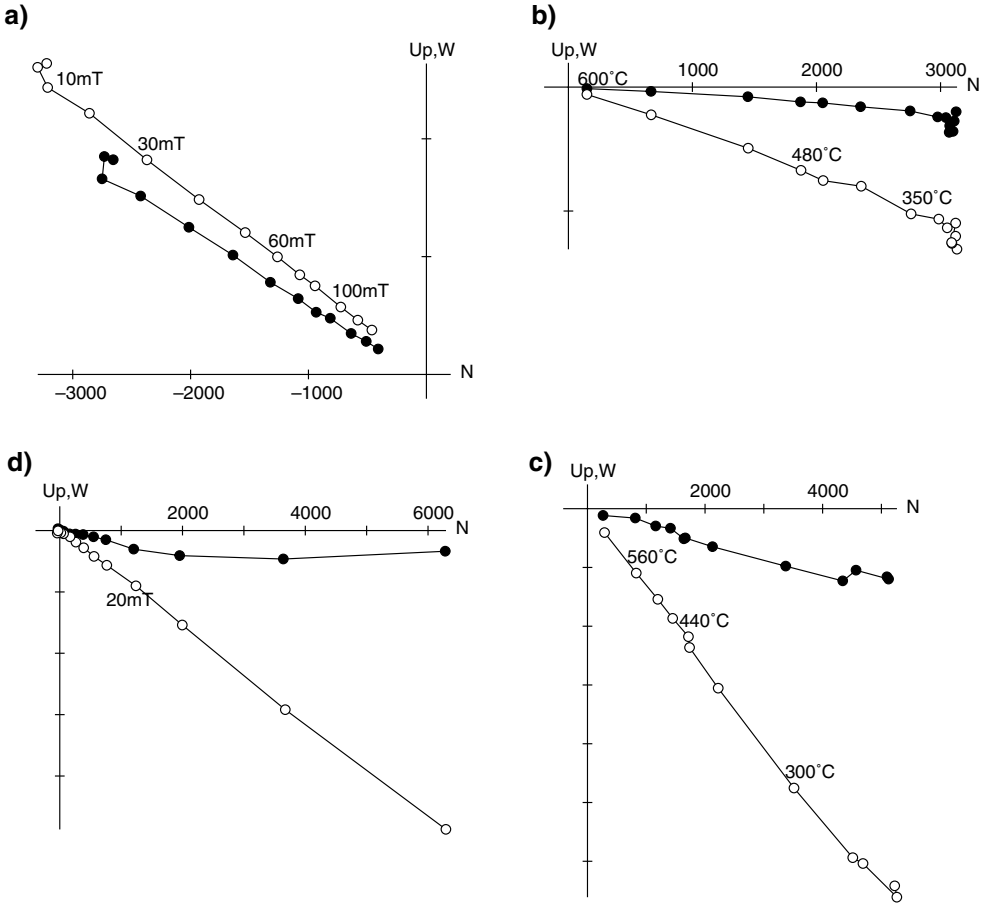

Fig. 2 Orthogonal projections of demagnetization data of specimens: **a** 223-2 of site LM-4, **b** 252-2 of site P-2, **c** 270-1 of site UM-1 and **d** 272-1 of site UM-3. Scales on the axes are given in mA/m. *Open symbols* correspond to projections on the vertical plane, *solid symbols* to the projection on the horizontal plane

analysis. For five samples a stable end point analysis was not suitable. Therefore, the great circle technique according to Mcfadden and McElhinny (1988) was applied. The mean directions for each lava flow were calculated using Fisher (1953) statistics (Table 1).

Directional results are analyzed ''in situ'' without bedding corrections, assuming that no major tilts affected the lavas since extrusion. Successively sampled lavas, obtained in profile P (Fig. 1), were tested for whether they recorded independent states of the geomagnetic field. In order to quantify the independency of successive directions we used the *F*-distribution test (e.g., Butler 1992). The probability to which successive flows are independent was calculated and for values less than 95% between flows, the lavas are assumed to have recorded the same geomagnetic field. These flows were then combined to a directional group DG (Table 1). This purely directional approach is supported by similar intensities for flows P-2 and P-3. For P-7 and P-8 this assumption is only based on directional results, for which the grouping is not completely unambiguous. Directional group calculation started from the lowest and, therefore, oldest flow in a succession.

Intermediate directions are defined by a difference between the Earth's rotation axis and the virtual geomagnetic pole (VGP) latitude of more than 35°, which is observed in two lava flows. Excluding those intermediate directions and using the two directional groups, the average mean direction corresponds to (Dec): 3.6°, (Inc): 38.7°, α_{95}: 6.2° which is similar to the local present day field. Within limits of uncertainty, the direction corresponds to that of an axial dipole field, showing a slightly far-sided effect. The VGP dispersion corrected for the within-site-scatter (McElhinny and McFadden 1997) results in S_f=16.5 with upper and lower confidence limits (Cox 1969) of S_{up}=21.4 and S_{low}=13.4. This dispersion is similar to the average for this latitude obtained for the last 5 Myr (McElhinny and McFadden 1997). Using not directional groups but individual lava flows for calculation of average parameters has no significant effect on the results.

Rock magnetics and paleointensity determination

Strong field thermomagnetic curves point to the presence of two different magnetic phases in the samples.

Table 1 Paleomagnetic results

Site	$Site_{long}$ (°E)	$Site_{lat}$ (°N)	n / N (N_{gc})	Dec (°)	Inc (°)	k	α_{95} (°)	VGP_{long} (°E)	VGP_{lat} (°N)	n_p / N_p	$F_w \pm \sigma_w$ (μT)	P
BC-1	343.130	28.319	6 / 5 (2)	340.4	25.7	97	8.4	218.1	66.5			N
BC-2	343.131	28.321	6 / 5	97.8	9.8	71	9.2	65.1	−4.5			I
C-1	343.143	28.320	5 / 4	21.0	30.7	113	8.7	100.0	67.3			N
C-2	343.142	28.323	4 / 4	24.5	56.0	322	5.1	45.1	67.8	4 / 4	18.4 ± 0.6	N
C-3	343.144	28.328	5 / 5	11.4	58.5	135	6.6	21.1	75.6			N
LM-1	343.140	28.293	4 / 4	161.7	−51.0	398	4.6	89.8	−73.8			R
LM-2	343.146	28.293	5 / 5 (2)	184.7	−38.3	104	8.1	309.8	−82.0			R
LM-3	343.148	28.296	4 / 4	175.5	−32.2	575	3.8	5.0	−78.4			R
LM-4	343.152	28.298	6 / 4	212.7	−38.1	370	4.8	258.8	−59.6	8 / 8	30.4 ± 0.7	R
LM-5	343.155	28.299	4 / 4	169.4	−31.1	513	4.1	25.7	−74.9	3 / 1	22.5	R
UM-1	343.160	28.308	6 / 5	11.5	39.6	129	6.8	99.9	78.1			N
UM-2	343.170	28.305	6 / 6	335.7	50.9	134	5.8	268.1	68.7			N
UM-3	343.176	28.300	5 / 5	19.3	52.6	441	3.6	52.0	72.7			N
P-1	343.145	28.344	5 / 5	322.9	−67.5	270	4.7	185.9	4.7			I
P-2	*343.145*	*28.344*	*4 / 4*	*1.8*	*23.3*	*512*	*4.1*	*156.9*	*73.7*	*4 / 3*	*25.1 ± 2.0*	*N*
P-3	*343.145*	*28.344*	*5 / 5*	*357.9*	*24.2*	*118*	*7.1*	*170.7*	*74.2*	*4 / 1*	*24.6*	*N*
DG: P-2, P-3			9 / 9	359.6	23.8	181	3.8	164.6	74.1	8 / 4	25.0 ± 1.4	N
P-4	343.145	28.344	5 / 5	10.4	26.7	100	7.7	126.8	72.8	4 / 3	15.5 ± 0.6	N
P-5	343.143	28.342	6 / 5 (1)	354.5	24.0	167	6.1	182.3	73.4			N
P-6	343.141	28.339	6 / 4	6.9	32.2	194	6.6	131.4	77.4			N
P-7	*343.141*	*28.339*	*4 / 4*	*355.0*	*38.6*	*962*	*3.0*	*198.8*	*82.0*			*N*
P-8	*343.143*	*28.342*	*4 / 4*	*358.2*	*35.4*	*113*	*8.7*	*174.1*	*81.1*			*N*
DG: P-7, P-8			8 / 8	356.6	37.0	201	3.9	185.8	81.7			N
P-9	343.141	28.339	4 / 4	5.6	22.5	136	7.9	144.6	72.6	4 / 4	19.8 ± 1.7	N
P-10	343.141	28.339	4 / 4	11.3	41.7	122	8.3	93.7	79.0			N
P-11	343.145	28.347	5/4	9.9	43.2	350	4.9	90.7	80.6	3/3	36.6 ± 0.7	N
TA-1	343.130	28.339	4 / 4	0.6	40.9	1703	2.2	156.7	85.1	4/3	27.6 ± 1.4	N
TA-2	343.118	28.348	5 / 5 (1)	184.7	−36.8	161	6.2	313.5	−81.1			R

Site mean inclinations and declinations, as well as the precision parameter k and α_{95} for sampled sites. n / N denotes the number of samples treated (n) versus the number of samples used (N) for calculating the site mean direction. The number of samples analyzed with great circles (N_{gc}) is given in brackets. Also shown are the VGP coordinates, amount of attempted (n_p)and successful (N_p) paleointensity determinations for individual drill cores, weighted mean paleointensity and the polarity P (R reversed, N normal and I intermediate). Directions were considered to represent intermediate polarity when the difference between the Earth's rotation axis and the VGP latitude was greater than 35°. Site locations were determined by GPS (WGS84). Individual units contained in directional groups (DG) are in italics

A Curie temperature (T_C) between 490 and 560°C is present in all specimens (Fig. 3a). During thermal demagnetization of sister specimens similar high unblocking temperatures bearing a characteristic remanent magnetization are found. Susceptibility variation, measured during thermal demagnetization, is generally very limited for samples showing such single T_C. This magnetic phase is interpreted as an exsolved titanomagnetite, which formed during high-temperature oxidation. A few specimens, 30% of the collection, showed an additional T_C range of 100–200°C. These low T_Cs are interpreted as being the result of predominantly unexsolved titanomagnetite grains. Samples containing this second phase usually exhibit significant alteration during heating experiments, leading to non-reversible thermomagnetic curves (Fig. 3b) and significant susceptibility variation during thermal demagnetization. Therefore, samples from these sites were excluded from paleointensity analysis.

Hysteresis curves are generally potbellied. Hysteresis parameters analyzed according to Day et al. (1977) indicated dominantly single domain to pseudo-single domain states for the magnetic minerals of the investigated samples. Determination of AMS revealed very small anisotropy factors $P < 1.03$.

Altogether 50 samples from 18 lavas were chosen for Thellier-type paleointensity determinations. Paleointensity experiments were only conducted on samples, which yielded the mean characteristic remanence direction of the flow. All selected samples contain fresh olivine crystals with no or limited traces of iddingsite indicating a minor or no influence of low-temperature alteration throughout the geological history (Smith et al. 1987). Successful results were obtained from 27 samples of 8 lavas. Some examples of accepted paleointensity determinations are shown in Fig. 4. The results and statistical parameters for successful determinations are listed in Table 2. If check correction was applied, the class in Table 2 was extended by a

Table 2 Paleointensity results from Teno

Site	*n* / *N*	Specimen	Type	T_{min} (°C)	T_{max} (°C)	N_p	*f*	*g*	*q*	*w*	Class	$H \pm \sigma$ (μT)	$F_w \pm \sigma_w$ (μT)
C-2	4 / 4	211-1	MT4	340	570	10	0.88	0.83	27.2	9.6	A*	17.4 ± 0.5	18.4 ± 0.6
		211-2	MT4	100	580	13	0.96	0.78	20.7	6.2	A*	19.5 ± 0.7	
		211-3	MT4	370	570	9	0.86	0.83	40.1	15.1	A*	19.3 ± 0.3	
		211-4	MT4	200	570	11	0.88	0.81	14.8	4.9	A*	16.6 ± 0.8	
M-4	6 / 5	**223-1A**	**MT2**	**200**	**525**	**8**	**0.49**	**0.83**	**7.1**	**2.9**	**A**	**30.1 ± 1.7**	30.4 ± 0.7
		223-1C	**MT1**	**200**	**550**	**9**	**0.6**	**0.85**	**10.4**	**3.9**	**B**	**34.2 ± 1.7**	
		223-2	MT4	100	430	8	0.32	0.82	4.7	1.9	A	29.6 ± 1.7	
		223-3	MT4	200	530	10	0.5	0.85	6.7	2.4	B	29.1 ± 1.8	
		223-4	MT4	300	510	7	0.34	0.79	2.5	1.1	B*	28.2 ± 3.1	
		223-X	**MT2**	**300**	**500**	**6**	**0.44**	**0.79**	**5.3**	**2.6**	**B***	**32.4 ± 2.1**	
		223-X	**MT1**	**350**	**500**	**5**	**0.31**	**0.71**	**2.5**	**1.4**	**C**	**29.5 ± 2.6**	
M-5	3 / 1	224-4	MT4	250	490	8	0.34	0.81	4.6	1.9	A	22.5 ± 1.3	22.5
P-2 and P-3	8 / 4	252-1	MT4	200	510	10	0.4	0.88	9.5	3.4	B*	30.3 ± 1.1	25.0 ± 1.4
		252-2	MT4	200	600	12	0.91	0.86	18.9	6	B	24.0 ± 1.0	
		252-3	MT4	200	510	10	0.52	0.88	17.4	6.1	B	23.3 ± 0.6	
		251-3	MT4	100	490	10	0.65	0.87	12.7	4.5	B*	24.6 ± 1.1	
P-4	4 / 3	250-1	MT4	370	520	6	0.65	0.76	6.1	3.1	B	16.7 ± 1.4	15.5 ± 0.6
		250-2	MT4	380	570	7	0.9	0.76	10.2	4.6	B	15.5 ± 1.0	
		250-X	MT4	430	530	5	0.74	0.74	6.1	3.5	B*	14.6 ± 1.3	
P-9	4 / 4	261-1	MT4	200	410	6	0.46	0.76	12.2	6.1	A	16.0 ± 0.5	19.8 ± 1.7
		261-2	MT4	200	550	11	0.85	0.85	48.7	16.2	A*	17.9 ± 0.3	
		261-3	MT4	460	570	6	0.62	0.79	26.1	13.1	A*	22.7 ± 0.4	
		261-4	MT4	100	460	9	0.46	0.83	9.6	3.6	B	24.1 ± 1.0	
P-11	3 / 3	230-1	MT4	340	520	7	0.35	0.79	3.4	1.5	A	39.8 ± 3.2	36.6 ± 0.7
		230-2	MT4	370	570	9	0.74	0.83	28.1	10.6	A*	37.2 ± 0.8	
		230-4	MT4	340	570	10	0.86	0.84	43.6	15.4	B	35.9 ± 0.6	
TA-1	4 / 3	216-1	MT4	340	510	7	0.33	0.75	4.7	2.1	B	30.4 ± 1.6	27.6 ± 1.4
		216-2	MT4	300	480	6	0.35	0.78	2.1	1.1	B*	32.4 ± 4.2	
		216-3	MT4	340	570	10	0.88	0.86	28.8	10.2	B*	26.5 ± 0.7	

n / *N* shows attempted versus successful paleointensity determinations. T_{min} and T_{max} specify the temperature range of the straight-line segment calculated over N_p successive points. The fraction of the NRM (*f*), the gap factor (*g*) and the quality factor (*q*) were calculated according to Coe et al. (1978). *w* denotes the weighting factor of Prévot et al. (1985). Class defines excellent (A) or good (B) quality according to the criteria. One class C results was accepted, since all criteria except δ_{pal} (Leonhardt et al. 2004a), which slightly exceeded the class B threshold, satisfied class A. A superscripted star added to the class indicates alteration corrected analysis. *H* and F_w are the paleointensity values with associated standard deviation (σ) for the individual determination and the weighted site mean, respectively. The results indicated in bold are from the same drill core and were averaged before calculating the site mean

superscripted star. Check corrected and non-corrected determinations yield similar results for the lavas. For site C-2, only check corrected results are listed in Table 2. Non-check corrected analysis would lead to a similar mean value with a higher standard deviation. The fraction of NRM, however, would be below 30% for all analyzes and therefore not conform with the applied criteria. A weighted site mean value was calculated using the weighting factor *w*. Due to the quality differences of individual determinations, a weighted standard deviation (SD_w) was determined despite the fact that mathematically speaking it is not correct as the weight is not determined according to the theory of errors. Two specimens were measured from drill cores 223-1 and 223-X (site M-4), respectively, showing in both cases, within the limits of uncertainty, the same mean values for the drill core. For calculation of the mean value of this site, the multiple measurements of one drill core were averaged before calculating an overall site mean from independent drill core results. With the exception of site M-5 at least three independent results were obtained for each lava flow or DG, showing a within-site-scatter well below 10%.

The average intensity, determined by an arithmetic mean over all sites corresponds to 24.5 ± 6.9 μT, which results in a virtual axial dipole moment (VADM) of $(4.9 \pm 1.4) \times 10^{22}$ A m^2.

Discussion

Structural and temporal evolution of the Teno massif

Paleomagnetic results in combination with published radiometric age determinations allow a more detailed reconstruction of the temporal evolution of the Teno

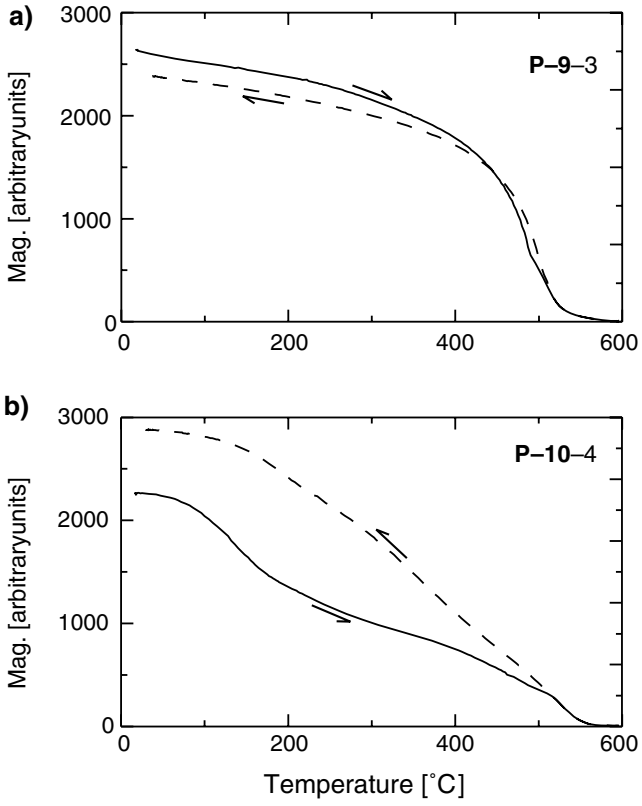

Fig. 3 Thermomagnetic curves. *Solid lines* show heating cycles, *dashed lines* cooling cycles. Part **a** shows an almost reversible curve with Ti-poor titanomagnetite as dominating magnetic mineral, **b** a second magnetic phase with T_C of ~ 180°C is present in the heating cycle, which is less developed during subsequent cooling. This observation and the increased magnetization during cooling are interpreted as an oxidation of a primary Ti-rich titanomagnetite during the heating/cooling cycle

volcano. A magnetostratigraphy for Teno is established by stratigraphically analyzing the paleomagnetic results in dependency of their age constraints defined by K/Ar and Ar/Ar age determinations.

The stratigraphically lowest and oldest formation, the MF, was dated to 6.42 and 6.02 Ma (Thirlwall et al. 2000), as well as 6.11 and 5.99 Ma (Guillou et al. 2004) which corresponds to an average age of 6.14 ± 0.20 Ma. Paleomagnetic sites M-1 to M-5, which clearly correspond to the MF, reveal reverse directions throughout. Comparison of the age/polarity relationship with the geomagnetic polarity timescale (GPTS; Cande and Kent 1995) indicates that this formation formed during the reverse chron C3An.1r lasting from 6.27 to 6.14 Ma (Fig. 5). All sites which presumably belong to the later subhorizontal CF (C-1, C-2, TA-1, UM-1) revealed normal polarity. Sites from EPF, consisting of subhorizontal flows as is the case for CF, are predominantly normally magnetized, ranging from stratigraphically low sites (300 m above sea level, profile P) up to very high altitudes of 800 m (C-3) and 1,070 m (UM-3). Ages for normally magnetized lavas of EPF are 6.11 Ma (Thirlwall et al. 2000), as well as 5.92 and 5.67 Ma (Guillou et al. 2004), resulting in an average age of 5.90 ± 0.22 Ma. A single reversely magnetized direction was published for a site sampled at an altitude of 1,330 m and dated to 5.54 Ma (Guillou et al. 2004), which according to Walter and Schmincke (2002) is part of the EPF. By far most of the > 1,000 m thick EPF, however, is normally magnetized and thus formed within less than 0.2 Myr. Therefore, it appears unlikely that the build-up of this formation extended far into the later reverse polarity chron. Hence, we conclude that the lavas of CF and EPF evolved dominantly during the normal polarity chron C3An.1n between 6.14 and 5.89 Ma (Fig. 5). Only the top of the present day formation was formed at the beginning of the later reverse chron C3n.4r. The two major sector collapses, MC and CC, both occurred during the normal polarity interval C3An.1n. Lavas of the LGF again show normal polarity throughout with ages of 5.15, 5.25 and 5.54 Ma (Guillou et al. 2004) resulting in an average of 5.31 ± 0.2 Ma. Comparisons with the GPTS show that these lavas were extruded during the "Thvera" normal polarity interval C3n.4n. between 5.23 and 4.98 Ma (Fig. 5). An almost complete absence of inverse directions between the LGF and the preceding EPF, is interpreted as a hiatus in volcanic activity during the inverse chron C3n.4r (5.89–5.23 Ma).

The fast evolution of the individual formations of the Teno massif as documented by radiometric ages and the agreement with the polarity timescale indicate that it is very unlikely that polarity intervals were missed due to limited sampling coverage. In-field fluxgate measurements to determine the NRM of unsampled rocks, which were conducted along the sampled profiles of this study and also along several other profiles by Guillou et al. (2004) further support the absence of additional polarity intervals.

The overall duration of volcanic activity corresponds to 1.2 Myr from 6.3 to 5.1 Myr, which is shorter than the 2.2 Myr duration suggested by Ancochea et al. (1990) based solely upon whole-rock K/Ar data. Nevertheless, the erosional phase already discussed by these authors appears to be present.

Our model for the temporal evolution is principally based on the same ages as considered by Guillou et al. (2004). Differences to their interpretation arise, as we give more weight to the magnetostratigraphic context. The basic stratigraphic evolution as suggested by these authors (Fig. 6 of Guillou et al. 2004) is, however, fully supported by our study. Our age constraints indicate

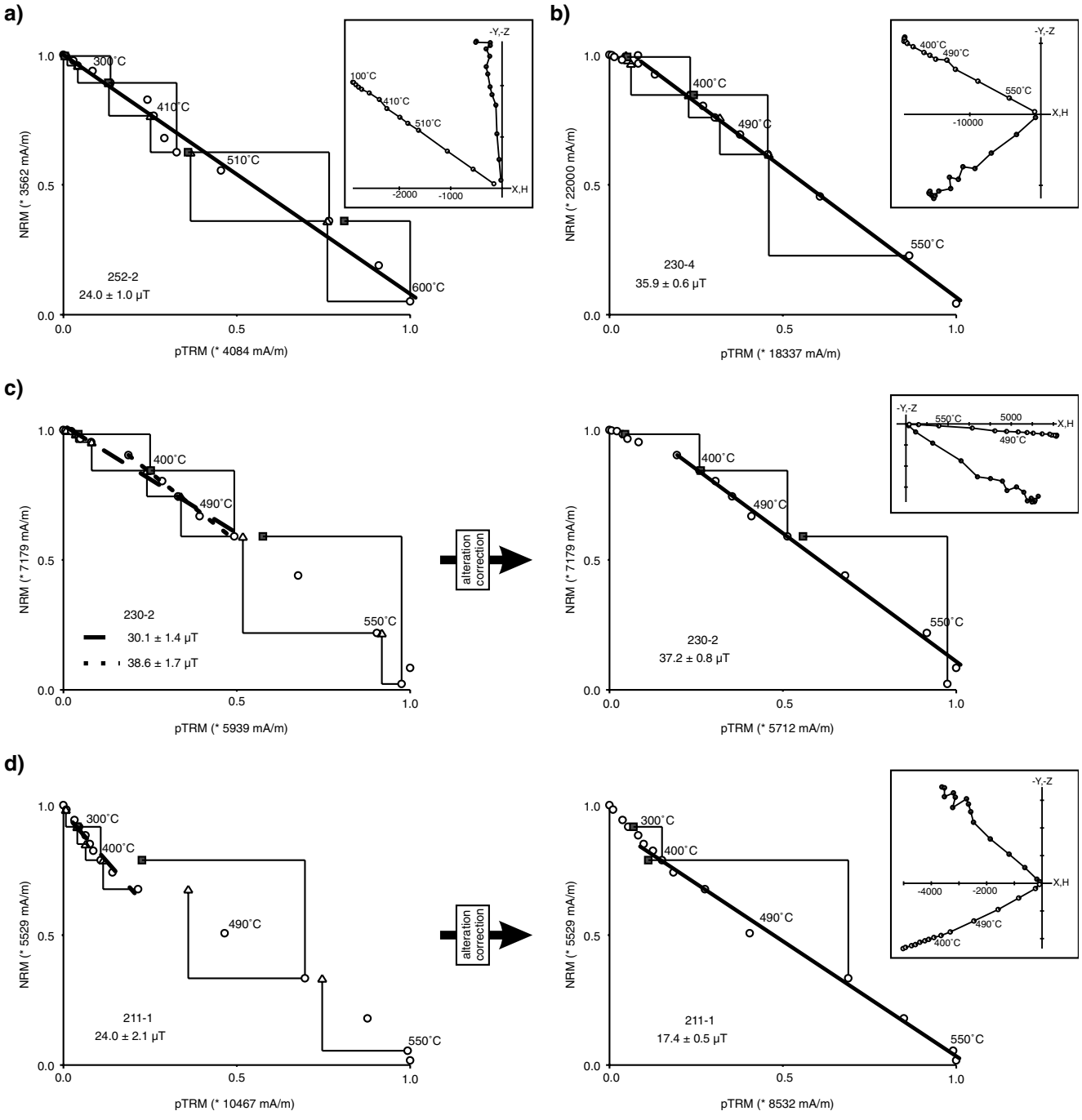

Fig. 4 NRM/pTRM diagrams. The straight-line segment is well defined and covers more than 50% of the NRM in 60% of the collection. *Triangles* indicate pTRM checks and *squares* denote additivity checks. The directional demagnetization behavior is shown in the orthogonal projection in the *upper right* of each plot. Part **a**, **b** show uncorrected analyzes. A corrected analysis of a specimen form the same lava as **b** is shown in **c**. Two different slopes could be used in the non-corrected low-temperature segment before the additivity check fails. After correction a slope covering 70% of the NRM is obtained with a similar intensity value as in **b**. An example of site C-2 with alteration affecting $T > 400°C$ is shown in **d**. After check correction, the additivity checks correspond to the pTRM value indicating successful correction (**c**, **d**)

that the two sector collapses and the successive infills of lavas exceeding a thickness of 700 m (Walter and Schmincke 2002) happened within 250 kyr. Repeated flank failures with 10–100 kyr periods are also observed in the Cañadas edifice (Ancochea et al. 1990; Cantagrel et al. 1999; Watts and Masson 2001), whereas post-collapse infill of lavas, however, is far less extensive.

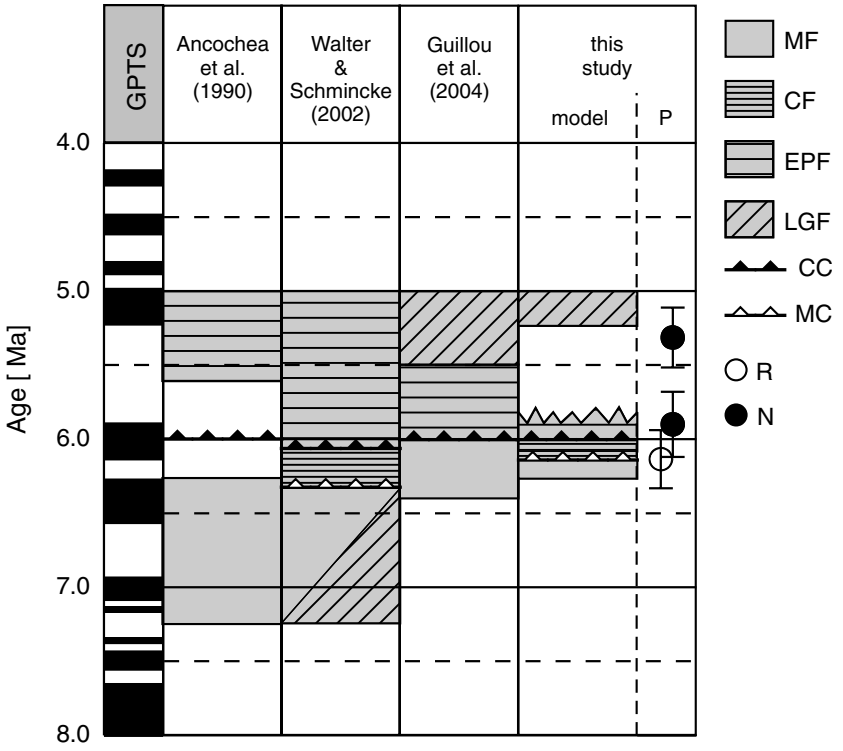

Fig. 5 Different models of evolutionary history of the Teno volcano. The abbreviations describing the formations as defined in this study are Masca Formation (*MF*), Carrizales Formation (*CF*), El Palmar Formation (*EPF*) and Los Gigantes Formation (*LGF*). The two major sector collapse events are denoted Masca collapse (*MC*) and Carrizales collapse (*CC*). Regarding the age constraints as given in the text, the obtained magnetic polarity data (*P*) are correlated to the GPTS (Cande and Kent 1995)

Considering the two sector collapses and assuming that the Teno volcano originally reached the dimensions of a conical structure of 1,500 m altitude and a diameter of 25 km, the average magma supply rate between 6.3 and 5.9 Ma can be estimated as approximately 1 km^3/kyr. Such a calculation is certainly not accurate and can be used only as a very rough estimate, as neither the original size of the volcano nor the volume removed by landslides and produced by infills can be correctly determined. Yet, this conservative value is comparable to the production rate estimated for the shield building phase of Gran Canaria (Mcdougall and Schmincke 1976; van den Bogaard and Schmincke 1998) and an order of magnitude lower than the rate for Hawaii (Moore and Clague 1992).

Thirlwall et al. (2000) pointed out that the Central shield and the Teno volcano are chemically very similar but originate from different mantle sources. The same authors conclude that Anaga lavas had a very distinctive source compared to the Teno, Central shield and Gran Canaria. Therefore, Teno and Anaga, despite their overlapping evolution time, must represent isolated volcanic edifices. The presence of a hiatus during the volcanic evolution of the Teno, similar to the typical evolutionary sequence of Hawaiian hotspot volcanoes, as well as the high production rate of magmas and the geochemical similarities to other Canary shield volcanoes indicate a hotspot-like origin for the Teno volcano. Two possible interpretations can be inferred from this observation: either the Teno represents an independent shield volcano or it represents a parasitic shield stage astride the rift zone of the central massif. The interpretation of the Teno edifice as a discrete hotspot shield volcano leads to an anomaly in age progression for the Canary Islands. According to the east-to-west age progression of the hotspot, the island of Gomera, which is located approximately 50 km west of the Teno massif, is supposed to be younger. The oldest volcanic rocks on this island were dated to ~ 9 Ma (Paris et al. 2005) and, thus, are almost 3 Ma older than the Teno volcano. The parasitic shield interpretation is supported by the position of the Teno edifice along a primary structural axis of Tenerife (Carracedo et al. 1998; Walter and Schmincke 2002).

Average late Miocene paleomagnetic field

The average age of the investigated lavas corresponds to 6.0 ± 0.2 Ma using the published radiometric age determinations of Thirlwall et al. (2000) and Guillou et al. (2004). The analysis of paleomagnetic directions results in a virtual pole position of VGP_{long}: 135.4°, VGP_{lat}: 82.9°, dp: 4.4°, dm: 7.4°. This pole position is slightly far-sided and right-handed as observed in many late tertiary lavas on the globe (e.g., Wilson 1970;

Kristjansson et al. 2003) and might be related to persistent multipole components of the geomagnetic field. The explicit reason for this often observed effect remains unclear. The average geomagnetic field intensity is approximately half of the present field intensity. Our obtained value is within the low-field level of the Earth's magnetic field (VADM: 4–5×10^{22} A m^2) as proposed by Shcherbakov et al. (2002) and Heller et al. (2003). Therefore, our data support the presence of a bimodal distribution of the geomagnetic dipole moment and indicate that a low-field state was maintained during the late Miocene.

Conclusion

1. Our magnetostratigraphic results provide additional information for the temporal evolution of the Teno volcano. An initial subaerial shield building stage took place during an reverse polarity period 6.3–6.1 Ma. Subhorizontal lavas were extruded after two major sector collapses and refilled the gaps. They are dominated by normal magnetizations over most of their succession indicating a rapid magmatism essentially from 6.1 to 5.9 Ma. After a period of quiescence within the following reverse polarity chron up to 5.3 Myr, normally magnetized lavas were again extruded.
2. The extrusion rates for the initial shield building stage, as determined from the above timescale, were fast, similar to the Gran Canaria shield basalts. Such high extrusion rates, the evolutionary sequence and the basic geochemical signature is similar as expected for hotspot volcanoes, like the Hawaiian prototype. Thus, we conclude that the 6.3 Ma Teno massif represents a parasitic shield volcano of the 12 Ma Central shield.
3. The late Miocene geomagnetic field average obtained from the sampled ~ 6.0 Myr old lavas of Teno is slightly far-sided/right-handed with respect to a geomagnetic axial dipolar field. The field strength is 40% lower than the present day value, similar to the mid-Miocene average and to the low-field state as suggested in a bimodal intensity distribution for the last 400 Myr. Therefore, our data support the presence of such low-field level in the late Miocene.

Acknowledgments We would like to thank the Medio Ambiente de Tenerife for sampling permission. We are particularly grateful to Juan Carlos Carracedo for his support prior and during the field work and his very helpful comments during preparation of this manuscript. We would like to thank Thomas Walter for his constructive review. Jürgen Matzka and Felix Hufenbecher are acknowledged for their field assistance. Suzan Emiroglu did part of the measurements. We profited from many discussions with David Krása and Christoph Heunemann. Sampling was funded by the German Science Foundation (So72/67-2,3).

References

Ancochea E, Fuster JM, Ibarrola E, Cendrero A, Coello J, Hernan F, Cantagrel JM, Jamond C (1990) Volcanic evolution of the island of Tenerife (Canary Islands) in the light of new K–Ar data. J Volcanol Geoth Res 44:231–249

Anguita F, Hernán F (1975) A propagating fracture model versus a hot-spot origin for the Canary Islands. Earth Planet Sci Lett 27:11–19

Anguita F, Hernán F (2000) The Canary Islands origin: a unifying model. J Volcanol Geoth Res 103:1–26

van den Bogaard P, Schmincke HU (1998) Chronostratigraphy of Gran Canaria. In: Weaver PPE, Schmincke HU, Firth JV, Duffield W (eds) Proceedings of the ODP, Scientific Results, vol 157, College Station, TX (Ocean Drilling Program), pp 127–140

Butler RF (1992) Paleomagnetism: magnetic domains to geologic terranes, 356. Blackwell Scientific Publications, Oxford

Cande SC, Kent DV (1995) Revised calibration of the geomagnetic polarity timescale for the late Cretaceous and Cenozoic. J Geophys Res 100:6093–6095

Cantagrel JM, Arnaud NO, Ancochea E, Fuster JM, Huertas MJ (1999) Repeated debris avalanches on Tenerife and genesis of Las Canadas caldera wall (Canary Islands). Geology 27:739–742

Carracedo JC (1979) Paleomagnetismo e historia volcanica de Tenerife. Aula de Cultura del Cabildo Insular de Tenerife, Tenerife, Espana, 82

Carracedo JC (1999) Growth, structure, instability and collapse of Canarian volcanoes and comparison with Hawaiian volcanoes. J Volcanol Geoth Res 94:1–19

Carracedo JC, Day SJ, Guillou H, Rodriguez Badiola E, Canas JA, Pérez Torrado FJ (1998) Hotspot volcanism close to a passive continental margin: the Canary Islands. Geol Mag 135:591–604

Coe RS, Grommé S, Mankinen EA (1978) Geomagnetic paleointensities from radiocarbon-dated lava flows on Hawaii and the question of the Pacific nondipol low. J Geophys Res 83:1740–1756

Cox A (1969) Confidence limits for the precision parameter *k*. Geophys J R Astron Soc 18:545–549

Day R, Fuller MD, Schmidt VA (1977) Hysteresis properties of titanomagnetites: grain size and composition dependence. Phys Earth Planet Inter 13:260–266

Fisher RA (1953) Dispersion on a sphere. Proc R Soc Lond A 217:295–305

Fuster JM, Araña V, Brandle JM, Navarro M, Alonso U, Aparicio A (1968) Geologia y Volcanologia de las Islas Canarias: Tenerife, 195. Instituto Lucas Mallada, Madrid

Guillou H, Carracedo JC, Pérez Torrado FJ, Rodriguez Badiola E (1996) K–Ar ages and magnetic stratigraphy of a hotspot-induced, fast grown oceanic island: El Hierro, Canary Islands. J Volcanol Geoth Res 73:141–155

Guillou H, Carracedo JC, Duncan RA (2001) K–Ar, ^{40}Ar–^{39}Ar ages and magnetostratigraphy of Brunhes and Matuyama lava sequences from La Palma Island. J Volcanol Geoth Res 106:175–194

Guillou H, Carracedo JC, Paris R, Pérez Torrado FJ (2004) Implications for the early shield-stage evolution of Tenerife from K/Ar ages and magnetic stratigraphy. Earth Planet Sci Lett 222:599–614

Heller R, Merrill RT, McFadden PL (2002) The variation of intensity of the Earth's magnetic field with time. Phys Earth Planet Inter 131:237–249

Heller R, Merrill RT, McFadden PL (2003) The two states of paleomagnetic field intensities for the past 320 million years. Phys Earth Planet Inter 135:211–223

Hoernle K, Schmincke HU (1993) The role of partial melting in the 15-Ma geochemical evolution of Gran Canaria: a blob model for the Canary hotspot. J Petrol 34:599–626

Juárez MT, Tauxe L, Gee JS, Pick T (1998) The intensity of the Earth's magnetic field over the past 160 million years. Nature 394:878–881

Krása D, Heunemann C, Leonhardt R, Petersen N (2003) Experimental procedure to detect multidomain remanence during Thellier–Thellier experiments. Phys Chem Earth 28:681–687

Kristjansson L, Hardarson BS, Aundunsson H (2003) A detailed palaeomagnetic study of the oldest (~15 Myr) lava sequence in Northwest Iceland. Geophys J Int 155:991–1005

Langenheim VAM, Clague DA (1987) The Hawaiian–Emperor volcanic chain. Part II. Stratigraphic framework of volcanic rocks of the Hawaiian Islands. In: Decker RW, Wright TL, Stauffer PH (eds) Volcanism in Hawaii. U.S. Geological Survey, Denver, pp 55–84

Leonhardt R, Soffel HC (2002) A reversal of the Earth's magnetic field recorded in mid Miocene lava flows of Gran Canaria: paleointensities. J Geophys Res 107:2299. DOI 10.1029/2001JB000949

Leonhardt R, Hufenbecher F, Heider F, Soffel H (2000) High absolute paleointensity during a mid Miocene excursion of the Earth's magnetic field. Earth Planet Sci Lett 184:141–154

Leonhardt R, Matzka J, Menor EA (2003) Absolute paleointensities and paleodirections from Fernando de Noronha, Brazil. Phys Earth Planet Inter 139:285–303

Leonhardt R, Heunemann C, Krása D (2004a) Analyzing absolute paleointensity determinations: acceptance criteria and the software ThellierTool4.0. Geochem Geophys Geosyst 5:Q12016. DOI 10.1029/2004GC000807

Leonhardt R, Krása D, Coe RS (2004b) Multidomain behavior during Thellier paleointensity experiments: a phenomenological model. Phys Earth Planet Inter 147:127–140

McDougall I, Schmincke HU (1976) Geochronology of Gran Canaria, Canary Islands: age of shield building volcanism and other magmatic phases. Bull Volcanol 40:57–77

McElhinny MW, McFadden PL (1997) Palaeosecular variation over the past 5 Myr based on a new generalized database. Geophys J Int 131:240–252

McFadden PL, McElhinny MW (1988) The combined analysis of remagnetization circles and direct observations in palaeomagnetism. Earth Planet Sci Lett 87:161–172

Moore JG, Clague DA (1992) Volcano growth and evolution of the island of Hawaii. Geol Soc Am Bull 104:1471–1484

Morgan WJ (1983) Hotspot tracks and the early rifting of the Atlantic. Tectonophysics 94:123–139

Paris R, Guillou H, Carracedo JC, Pérez Torrado FJ (2005) Volcanic and morphological evolution of La Gomera (Canary Islands) based on new K/Ar ages and magnetic stratigraphy: implications for oceanic islands evolution. J Geol Soc Lond 162:1–16

Prévot M, Mankinen EA, Coe RS, Grommé S (1985) The Steens Mountain (Oregon) geomagnetic polarity transition 2. Field intensity variations and discussion of reversal models. J Geophys Res 90:10417–10448

Riisager P, Riisager J (2001) Detecting multidomain magnetic grains in Thellier paleointensity experiments. Phys Earth Planet Inter 125:111–117

Schmincke HU (1973) Magmatic evolution and tectonic regime in the Canary, Madeira, and Azores Islands groups. Geol Soc Am Bull 84:633–648

Schmincke HU (1979) Age and crustal structure of the Canary Islands. J Geophys 46:217–224

Selkin PA, Tauxe L (2000) Long-term variations in paleointensity. Philos Trans R Soc Lond 358:1065–1088

Shcherbakov VP, Solodovnikov GM, Sycheva NK (2002) Variations in the geomagnetic dipole during the past 400 million years (Volcanic rocks). Izv Acad Sci USSR Phys Solid Earth Engl Trans 38:113–119

Smith KL, Milnes AR, Eggleton RA (1987) Weathering of basalts: formation of iddingsite. Clays Clay Miner 35:418–428

Thirlwall MF, Singer BS, Marriner GF (2000) ^{39}Ar–^{40}Ar ages and geochemistry of the basaltic shield stage of Tenerife, Canary Islands, Spain. J Volcanol Geoth Res 103:247–297

Valet JP, Brassart J, Le Meur I, Soler V, Quidelleur X, Tric E, Gillot PY (1996) Absolute paleointensity and magnetomineralogical changes. J Geophys Res 101:25029–25044

Valet JP, Brassat J, Quidelleur X, Soler V, Gillot PY, Hongre L (1999) Paleointensity variations across the last geomagnetic reversal at La Palma, Canary Islands, Spain. J Geophys Res 104:7577–7598

Walter TA (2003) Buttressing and fractional spreading of Tenerife, an experimental approach on the formation of rift zones. Geophys Res Lett 30:1296. DOI 10.1029/2002GL016610

Walter TR, Schmincke HU (2002) Rifting, recurrent landsliding and Miocene structural reorganization on NW-Tenerife (Canary Islands). Int J Earth Sci (Geol Rundsch) 91:615–628

Watts AB (1994) Crustal structure, gravity anomalies and flexure of the lithosphere in the vicinity of the Canary islands. Geophys J Int 119:648–666

Watts AB, Masson DG (2001) New sonar evidence for recent catastrophic collapses of the north flank of Tenerife, Canary Islands. Bull Volcanol 63:8–19

Watts AB, Peirce C, Collier J, Dalwood R, Canales JP, Henstock TJ (1997) A seismic study of lithospheric flexure in the vicinity of Tenerife, Canary Islands. Earth Planet Sci Lett 146:431–447

Wilson RL (1970) Permanent aspects of the Earth's non-dipol magnetic field over the Upper Tertiary times. Geophys J R Astron Soc 19:417–437